Assembling metal-organic cages as porous materials

Elí Sánchez-González,[a,b] Min Ying Tsang,[a,c] Javier Troyano,[a] Gavin A. Craig*[d] and Shuhei Furukawa*[a]

Received 00th January 20xx,
Accepted 00th January 20xx

DOI: 10.1039/x0xx00000x

There is growing interest in metal-organic cages (MOCs) as porous materials owing to their processability in solution. The discrete molecular character and surface features of MOCs have a direct impact on the interactions between cages, enabling the final physical state of the materials to be tuned. In this tutorial review, we discuss how to use MOCs as core building units, highlighting the role played by surface functionalisation of MOCs in leading to porous materials in a range of states covering crystalline solids, soft matter, liquids and composites. We finish by providing an outlook on the opportunities for this work to serve as a foundation for the development of increasingly complex functional porous materials structured over various length scales.

Key learning points

1. Metal-organic cages (MOCs) are discrete molecules that enclose a potential volume of empty space within the molecule. The selection of inorganic building units and design of organic ligands can be used to retain a specific cage geometry and internal pore, while varying the functionality and possible reactivity of the MOC surface.

2. The surface functionality of MOCs regulates the intercage interactions, enabling the formation of crystalline and amorphous solids, liquids, composites and soft matter based on MOCs.

3. The porosity of MOC-based materials arises from the combination of the intrinsic porosity of the cage and the extrinsic porosity generated by spatial organisation of the cages in the final assembled state.

1. Introduction

To fulfil industrial applications, advanced materials must be processable. While functional materials can show superb performance in as-synthesised phases like powders, practical applications often require specific morphologies such as films, monoliths, tablets, colloids, fibres, foams, etc. or positioning on substrates.[1] Controlled assembly over specific length scales may also be necessary, either at the nanoscale (submicron) for electronic or biological applications or over much longer scales for mass-fabrication or mechanical applications.

These requirements apply to porous materials, which are used in a myriad of applications such as sensing, optics, fine molecular separations, catalysis, energy storage and conversion.[2-4] As well as classical porous materials including zeolites and activated carbons, metal-organic frameworks (MOFs) are of great importance. The pore size and shape found in the two- or three-dimensional extended structures of MOFs are tunable through the use of modular building blocks (metal clusters and organic linkers).[3] Because crystallisation occurs at the same time as the building blocks assemble, MOFs are often processed *in situ* during synthesis. For instance, the fabrication of MOF-based membranes or superstructures can be achieved by direct crystallisation in target environments. In this case, the focus is on how solutions of precursor organic ligands and metal sources are mixed to control the crystallisation, or how heterogeneous nucleation may be induced by locally changing reaction conditions. An exception to these approaches is chemical vapour deposition, in which vapours of the organic components are reacted with metal oxides that have been deposited on a substrate.[5]

One method to achieve solution processability in MOFs is to develop "soluble" MOF nanocolloids,[6] which can be further processed to form composite materials.[7] However, there are still processability challenges for MOF-based colloids in size control, monodispersity and colloidal stability. The nature of extended network structures only allows MOFs to be stable as dispersible nanocrystals measuring tens of nanometers in size.[6] The extreme case of downsizing a MOF would lead to a single pore unit. This single pore unit corresponds to the intrinsic cavity found in metal-organic cages (MOCs).[3] Since the seminal work of Saalfrank, Fujita, Stang, and others, most of the chemistry of MOCs has been developed in the solution phase.[8-11] For use as porous materials in the solid-state, MOCs must be thermally and chemically stable, such that the intrinsic pore of the cage is retained even after the removal of solvents from the structure.[12] The stability of the individual cage can be regulated

[a] *Institute for Integrated Cell-Material Sciences, Kyoto University, Yoshida, Sakyo-ku, Kyoto 606-8501, Japan.*
[b] *Laboratorio de Fisicoquímica y Reactividad de Superficies (LaFReS), Instituto de Investigaciones en Materiales, Universidad Nacional Autónoma de México, Circuito Exterior s/n, CU, Coyoacán, Ciudad de México 04510, Mexico.*
[c] *Advanced Materials Engineering and Modelling Group, Faculty of Chemistry, Wrocław University of Science and Technology, Wrocław, 50-373, Poland.*
[d] *Department of Pure and Applied Chemistry, University of Strathclyde, 295 Cathedral Street, Glasgow, G1 1XL, United Kingdom.*

† Footnotes relating to the title and/or authors should appear here.
Electronic Supplementary Information (ESI) available: [details of any supplementary information available should be included here]. See DOI: 10.1039/x0xx00000x

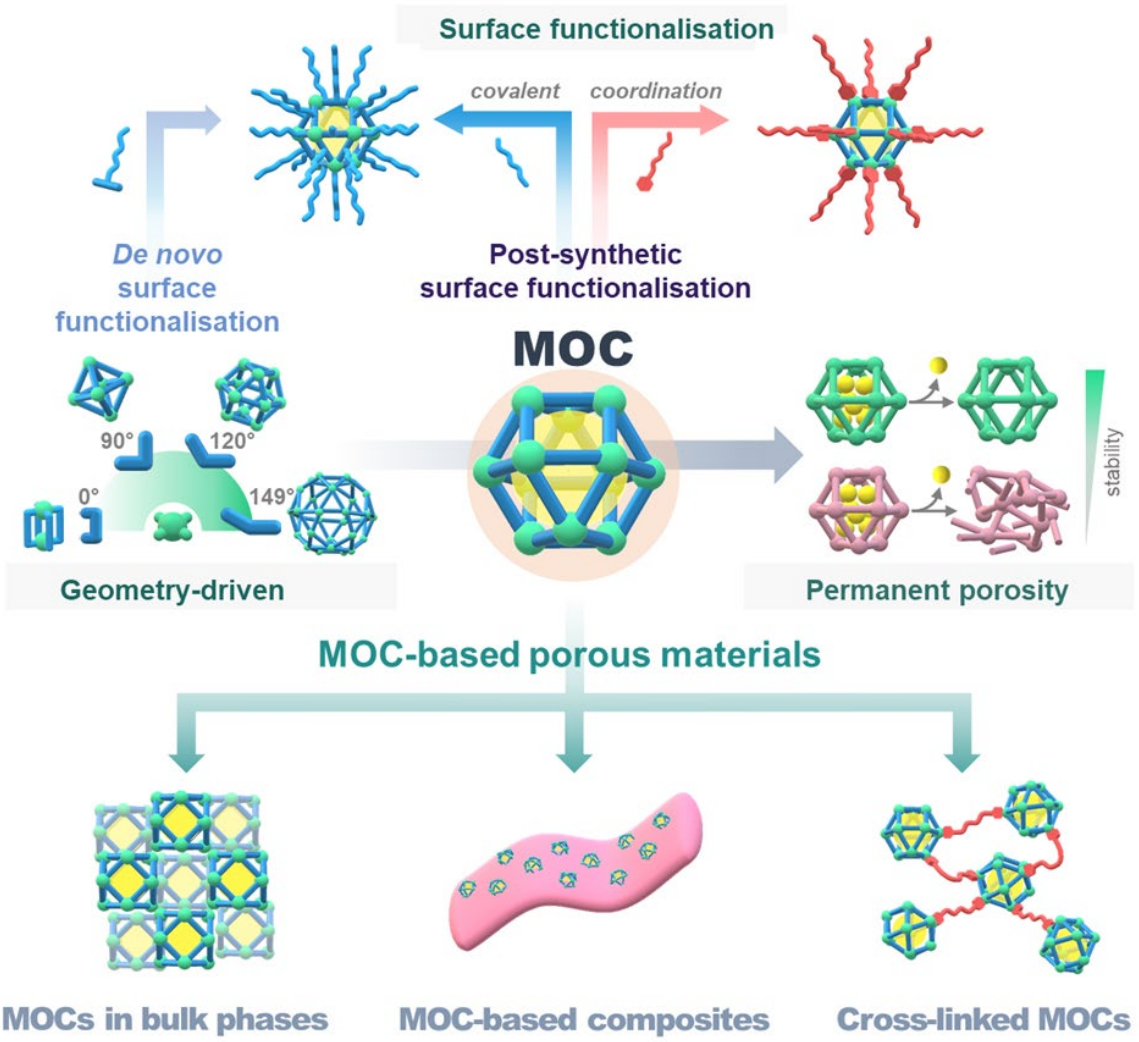

Fig. 1 (top) The synthetically tuneable features of metal-organic cages (MOCs): geometry-driven design, permanent porosity, and surface functionalisation (*de novo* and post-synthetic). (bottom) Assembly routes to synthesise MOC-based porous materials.

by the appropriate choice of metal ions and organic ligands. Chemical functionalisation of MOC surfaces can modulate their solubility and intermolecular interactions.[13] Here, MOCs offer an advantage over MOFs: the weak, reversible intermolecular interactions in MOCs favour their solubility, and from solution phases the individual cages can be processed into a wide range of porous materials. For example, this approach can be used to direct the assembly of MOCs into hierarchically porous structures, combining the intrinsic microporosity of the cage with the intermolecular extrinsic porosity generated by arrangement of the MOCs in the solid state. Because the MOC provides a microporous unit, there is no requirement for MOC-based materials to display long-range order for accessible porosity. This structural freedom enables the synthesis of soft or amorphous materials with well-defined porosities.

During the preparation of this manuscript, detailed reviews on specific aspects of MOCs were published reflecting the growing interest in these cage molecules.[12, 14-16] With this tutorial review, we provide a more general point of entry to this expanding area of research through a perspective on the fundamental approaches to assembling porous MOC-based materials. We identify the key design features of MOCs and their role in the porosity of the materials. We describe how the surface functionality of MOCs is the basis for using these cages as processable molecular building blocks in the synthesis of porous materials in forms including powders, liquids, thin films, and shapeable soft matter. Throughout, we highlight where a more specialist review is available, for example on the challenges in determining the surface areas of the cages,[12] or their role in the fabrication of soft matter.[17] Throughout the text, we refer to these molecules as MOCs, although readers may find that in the original reports they are referred to as metal-organic polyhedra (MOPs) or MOCs or porous coordination cages.

2. Why are MOCs suitable building blocks for porous materials?

The porosity, and mechanical and chemical stability of MOC-based materials are strongly correlated to both the characteristics of the cage and the assembly process of the material. Thus, they can be tuned by design. In the following subsections, we describe the design principles for individual MOC synthesis and their assembly protocols.

Synthetically tuneable aspects of MOCs

Similar to the design of porosity in MOFs, in which the network topology defines the pore shape, the inner cavity of MOCs can be designed by choosing the cage geometry. The combination of organic linkers of appropriate symmetry with metal ions/clusters drives the desired cage geometry and thus potential connectivity of the cage.[3, 14, 18] A review by Lee and co-workers describes the range of polyhedra that are accessible through considering these possible combinations.[14] An example of this is the formation of M_nL_{2n} Pd-based cages – their shape can be controlled almost precisely by the angle between the two bonding vectors of the two terminal pyridyl moieties of the ligand L. This control spans M_2L_4 lantern-type cages when the terminal pyridyl rings coordinate in a parallel fashion (0°) to the Goldberg polyhedron $M_{48}L_{96}$ (152°) (Figure 1).[19] Similar linker-guided geometry is possible in M_nL_n cages with carboxylate-type linkers.[20] Carboxylate ligands are used to obtain neutral cages, often with higher stability in the solid-state than cationic cages containing neutral ligands. This stability is needed for permanent porosity, as MOCs should undergo activation – the procedure through which solvent molecules are removed from the structure of the MOCs – without their structural decomposition (Figure 1).

An important consideration in designing MOCs that can be fabricated into porous materials is to incorporate moieties that can be used as reactive nodes for post-synthetic modification. In this sense, MOCs have been described as hollow nanoparticles, where the exterior of the MOC corresponds to the nanoparticle surface. Albalad and co-workers have highlighted the opportunities for post-synthetic modification that are made possible by the "latent reactivity" of discrete MOCs.[21] The installation of functional groups in the ligand backbone is a general strategy to change the surface functionality of the cage. Such modifications can be performed by *de novo* synthesis of the linker or by post-synthetic modification of the cage (Figure 1). This reactive functional group is expected to form new covalent bonds. Another strategy is to use additional coordination sites on the metal ions/clusters while maintaining the coordination bonds that hold the MOC together. These coordination sites can be occupied initially by a terminal solvent molecule, which can be further replaced with a reactive linker to connect MOCs.[13, 22] A notable example of this surface modification of MOCs was demonstrated using cuboctahedral $[Rh_{24}(bdc)_{24}]$ cages based on dirhodium paddlewheel nodes as a platform for both covalent-based and coordination-based post-synthetic modification (bdc = 1,3-benzenedicarboxylate).[13] A variety of monotopic N-donor ligands were substituted into the axial position of the paddlewheels. This strategy was used to induce the solubility of cages that were otherwise in suspension, or even introduce chiral functionality in the case of coordination of *L*-proline. Through the combination of coordination and covalent functionalisation, the hydrophobicity of the cages was tuned, which would enable the MOCs to be used as building blocks in a wide variety of assembly conditions.

Assembly routes for porous materials based on MOCs

The synthetically tuneable aspects of MOCs highlighted above lend themselves to three principal approaches to the synthesis of MOC-based porous materials (Figure 1). The first is the synthesis of bulk phase materials, in which the intermolecular interactions between MOCs lead to the formation of crystalline or amorphous solids. As we will discuss in **Section 3**, the activation of the cages is challenging because the removal of solvent molecules from the MOC solids often drives the collapse of the MOCs into non-porous phases. Recent years have seen an increase in the description of approaches to attaining permanent porosity in these cages, which Gosselin and co-workers have observed through a greater number of reported surface areas for MOCs, as well as new record high surface areas being set.[12] We will highlight how solvent treatment plays a role in controlling the MOC packing and thus the resulting porosity of the cages. The synthetic tunability of the intercage interactions allows a full spectrum of materials to be obtained, running from crystalline phases through soft matter to, most recently, liquids.

The second approach is to embed the cages into a matrix to form a composite (**Section 4**). In this case, the cages can be dissolved and mixed with the matrix to achieve molecular-level dispersion, or particles of cage aggregates can be dispersed in a solvent and then mixed with a solution of the matrix prior to evaporation of the solvent to yield the composite. The challenges of this approach arise from the relative compatibilities of the MOCs and the matrix, solvents, and the potential for phase separation (aggregation of the cages or their particles within the matrix), leading to materials with compromised mechanical properties or poorer performance due to the formation of defects. Additionally, accessing the cage cavity is an ever-present challenge at the interface between cage and matrix. Often, the matrix can penetrate or block the cage windows and lead to loss of accessible porosity.

The third approach, covered in **Section 5**, is to connect pre-formed MOCs to form extended networks. Such cross-linking can be achieved by exploiting one or both of the different connection points that MOCs may offer: (1) coordinatively unsaturated metal sites and (2) reactive organic functional groups. Here, MOCs can be designed to present specific binding points and additionally, be combined with auxiliary linkers/metal ions. As highlighted by Khobotov-Bakishev and co-workers, cross-linking is emerging as one of the most versatile methods of using MOCs to access a range of porous matter, from crystalline networks to gels.[23] Further, the resulting extended structures can be tuned, for instance, by using rigid or

flexible additional linkers to attain highly regular or less well-defined extrinsic porosity, respectively.

3. Assembly of discrete MOCs in bulk phases

The synthesis of MOCs is commonly carried out in solution and the product may remain in solution or precipitate as crystalline or amorphous solids. The most common aim of the synthetic procedure is to obtain single crystals of the MOC that enable its chemical formula and geometry to be determined. In 2005, Yaghi and co-workers demonstrated gas uptake in MOCs for the first time in a series of Fe-based MOCs through gas sorption measurements.[24] This report also noted that two types of potential pore could be envisaged for these structures: the intrinsic porosity arising from the cavity of the MOC; and the extrinsic porosity from the space generated between cages. Although the design of the cages is used to control the intrinsic cage porosity, it is challenging to control the extrinsic porosity of these materials. The interactions between MOCs are exclusively non-covalent, consisting of combinations of van der Waals, π-π stacking, and hydrogen-bonding interactions, which are weaker than the coordination bonds that maintain the integrity of MOFs. The weak nature of these interactions has two consequences: (1) the removal of the solvent molecules that occupy the space between MOCs induces the modification of the cage packing, occasionally leading to amorphous phases; and (2) the cage can be recrystallised from different solvent media leading to many different solvent-driven packing arrangements of the MOC, which can lead to a single cage showing more than one type of gas uptake.

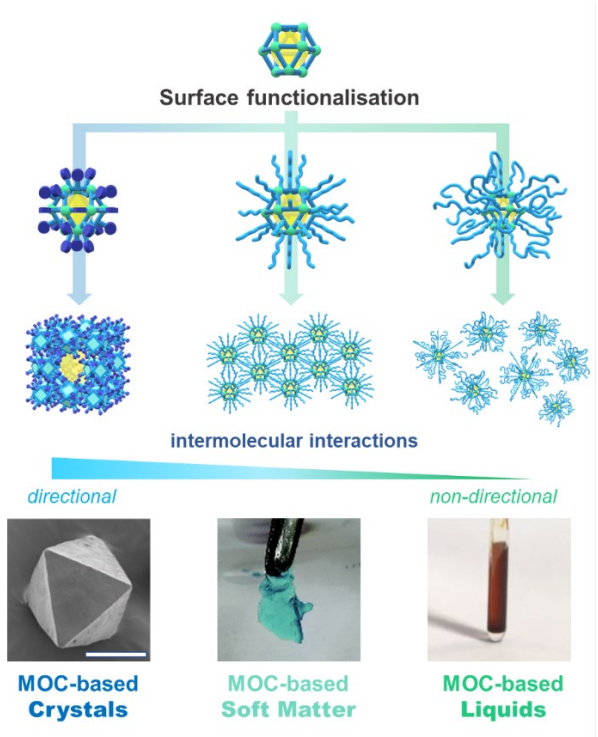

Fig. 2 (top) Surface functionalisation of metal-organic cages as means to modify their intermolecular interactions. Strongly directional interactions are more likely to induce the formation of highly ordered phases. (bottom) Examples of MOC-based materials in the bulk phase: SEM image from vanadium-based MOC, scale bar 100 μm (adapted with permission from ref. 26, Copyright 2018, John Wiley and Sons); a self-standing thin film of [Cu_{24}(th-bdc)$_{24}$] (reprinted from ref. 36 with permission from the Royal Society of Chemistry); the neat-liquid PEG-decorated Zn-based MOC (reprinted with permission from ref. 38, Copyright 2020, Springer Nature).

Crystalline structures

Considering each polyhedral cage as a tiling unit, the crystal structures of MOCs could be anticipated to be permutations of face-, edge-, or node-sharing polyhedra. Packing convex polyhedra is an optimisation problem for tiling 3D space, in which the cube and truncated octahedron are the only Platonic and Archimedean solids that can tile the space.[25, 26] Inefficient packing is therefore common to cage molecules, with solvent and/or counter-ions filling the intercage voids. In most cases, there is a lack of strongly directional intermolecular interactions to direct the crystal packing.

Surface modification of MOCs with functional groups can provide directional interactions to induce a denser and more stable packing (Figure 2). The broadest illustration of how the synthetic modification of the MOC surface affects crystal packing is provided by the family of cuboctahedral cages with the general formula [Cu_{24}(L)$_{24}$], where the metal nodes are based on copper(II) paddlewheel units and L is a derivative of isophthalate. Cages with small substituent groups (such as -Br, -OH, -OEt or -tBu)[22, 27-29] exhibit body-centred cubic packing, interacting with eight adjacent cages through van der Waals interactions. Bulkier substituents can increase the distance between cages and/or alter the packing of the molecules. For a series of alkoxy substituents, the intercage distance was found to increase upon increasing the chain length from ethoxy- to butoxy-functionalised ligands, while retaining bcc packing.[29] In contrast, hexagonal close packing was observed for the pentoxy-functionalised cage.[29] Appending an even bulkier group such as dodecoxy- chain induced an adamantanoid-like packing.[30] The long alkyl chains reduce the contact between neighbouring cages, leading to only four adjacent cages. In most cases, achieving this control over inter-cage interactions is not trivial. Nevertheless, individual MOCs can be regarded as tectons with specifically tailored surfaces.

Alternatively, inter-cage interactions in crystalline phases of MOCs can be tuned using post-synthetic modification. W. M. Bloch and co-workers described the reaction of the primary amines o-toluidine and 9-ethyl-9*H*-carbazol-3-amine with the aldehyde groups of the lantern-type MOC [Cu_4(CHO-L)$_4$] (L = 3,3'-((1,3-phenylene)bis(ethyne-2,1-diyl))dibenzoate).[31] As observed in the crystal structures, the main effect of these modifications was to increase the distance between the cages. The authors also suggested that through the judicious introduction of functional groups it is possible to control the rigidity of the structures and to decrease the influence of solvent molecules on the cage packing.

Crystalline phases of MOCs usually present solvatomorphs, obtained by different synthetic conditions or post-synthetic solvent processing. Polar solvents can interfere in hydrogen bond formation between MOCs, determining the interactions between cages.[32] D. Yan and co-workers reported a family of

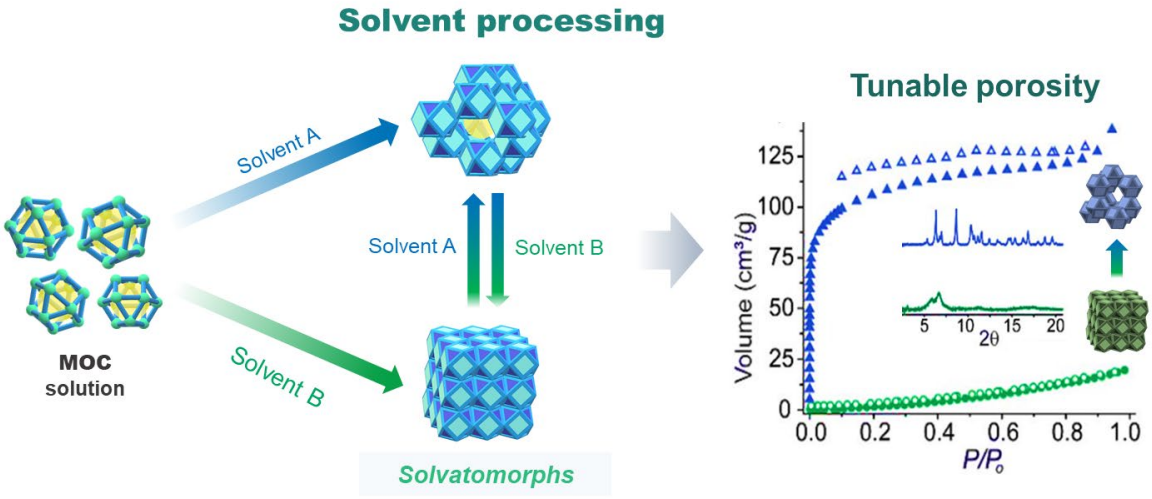

Fig. 3 Solvent processable metal-organic cages with tunable porosity. Solvatomorph A corresponds to the "open phase" and B the "closed phase". (right) Nitrogen sotpyion isotherms at 77 K measured for the solvatomorphs of $[Cu_4(COH\text{-}L)_4]$ showing on/off porosity. Inset PXRD patterns for activated (green) and solvated (blue) phases. Adapted from ref. 31 with permission from the Royal Society of Chemistry.

zirconocene-based tetrahedral MOCs which form extended arrays of hydrogen bonds.[33] The MOC $[(Cp_3Zr_3O(OH)_3)_4(btc)_4]Cl_4$ (ZrT-2), could be synthesised as two solvatomorphs, ZrT-2-α and ZrT-2-β, containing DMF or DMA, respectively (Cp = cyclopentadienyl; btc = 1,3,5-benzenetricarboxylate).[34] The difference in the ability of DMF and DMA to form hydrogen bonds induced two different solid-state packing arrangements of the chemically identical cages. As a result of a higher degree of intermolecular interactions, ZrT-2-β displayed a more robust packing arrangement that was retained upon thermal activation. The consequence was that the N_2 uptake at 77 K for ZrT-2-β was twice that observed for ZrT-2-α, ~300 and ~160 cm^3/g, respectively. This difference is due to the retention of the extrinsic porosity by ZrT-2-β, while the adsorption observed for ZrT-2-α is associated with the cage porosity.

These solvent effects can also be induced by post-synthetic solvent processing (Figure 3). This was found to be the case for an ethoxy-functionalised lantern-type cage $[Cu_4(EtO\text{-}L)_4]$ (L = 3,3'-((1,3-phenylene)bis(ethyne-2,1-diyl))dibenzoate).[35] The MOC was initially obtained from synthesis in DMF, and subsequent to solvent exchange with MeOH the activated lantern-type cage showed gate-opening behaviour in the CO_2 sorption isotherms recorded at 195 K. Recrystallisation of the activated phase from THF induced a distinct crystal packing, which under activation led to a rigid phase that presented Type I uptake of CO_2. The MeOH-exchanged sample exhibits a flexible packing which allows a higher CO_2 uptake compared to the rigid THF-exchanged sample, 12 and 7 moles of CO_2 per mole of MOC, respectively. Solvent processing could be used to cycle between these flexible and rigid phases. Furthermore, W. M. Bloch and co-workers reported that the porosity of an aldehyde-functionalised lantern MOC $[Cu_4(CHO\text{-}L)_4]$ was switched completely "on" and "off" through solvent processing (Figure 3).[31] The Initial solvatomorph, closed phase (1B), exhibited a low N_2 uptake at 77 K (~19 cm^3/g) while submerging it in MeOH prior to activation triggered a packing rearrangement resulting in the open phase (1A) with a higher N_2 uptake (~139 cm^3/g).

Soft matter

The introduction of long alkyl chains on the surface of MOCs is a widely-used strategy to increase the solubility of cages.[30] While the incorporation of bulky or long substituent groups on the surface of MOCs leads to loss of directional intercage interactions, causing a decrease in the crystallinity of the materials, it can open routes to soft matter. Some of the specific potential applications of this research direction include uses in batteries and soft robots, as summarised by Jahović and co-workers.[17] Omoto *et al.* described the use of bulky paraffinic substituents in the cuboctahedral cage $[Cu_{24}(th\text{-}bdc)_{24}]$, which could form a self-standing thin film (th-bdc = 3',4',5'-Tris(hexadecyloxy)-[1,1'-biphenyl]-3,5-dicarboxylate) (Figure 2).[36] Diffraction experiments showed that the film was not completely amorphous, but that the MOCs were arranged in a body-centred cubic packing arrangement forming a liquid crystal. Although the core of this MOC is the archetypal cuboctahedral MOC, the authors did not report gas sorption measurements: the distance between the cages suggests that the paraffinic groups may be intertwined thus hindering access to the pore of the cage. Reconciling the use of bulky linkers and the accessibility of the pores is a current challenge in the synthesis of porous soft matter based on MOCs.

Soluble MOCs might present opportunities to be processed directly into porous membranes. For this, Langmuir-Schaeffer (LS) or Langmuir Blodgett (LB) techniques were used to form dense monolayers of $[Rh_{24}(C_{12}\text{-}bdc)_{24}]$ (C_{12}-bdc = 5-dodecoxybenzene-1,3-dicarboxylate).[37] The hydrophobicity of the aliphatic chains aided the dispersion of the MOCs on the surface of water, leading to the formation of monolayers of *ca.* 2.5 nm in thickness. Neat MOC membranes were obtained by layer-by-layer deposition on a poly(1-trimethylsilyl-1-propyne) (PTSMP) substrate. The deposition of MOC thin films improved

the selectivity by two-fold (from approximately 4 to 8) for the separation of 10/90 CO_2/N_2 mixtures when compared to neat PTMSP membranes. These results showed the potential for the fabrication of neat MOC thin films, using a technique (LB) that can be scaled to obtain large-area membranes.

Liquids

With the appropriate design of the ligands, the synthetic tunability of MOCs could enable the synthesis of porous liquids, particularly Type 1 porous liquids – neat materials where no solvent is required to keep the porous entity in the liquid state. The challenge associated with these materials is to balance the weaker intermolecular interactions required for the cage to form a liquid at room temperature while preventing bulky functional groups or counter-ions from blocking the entry of gas molecules into the cavity of the cage. Other techniques can be used to probe the porosity of soft matter and liquids, such as NMR or positron annihilation lifetime spectroscopy (PALS). T.D. Bennett, J.R. Nitschke and co-workers designed a series of poly(ethylene) glycol-decorated tetrahedral MOCs assembled with Zn(II) nodes.[38] The poly(ethylene) glycol (PEG) units were terminated with imidazolium rings to prevent the extended chains from entering the cage. A longer PEG-based derivative, containing 20 repeating units, was obtained as a dark yellow viscous liquid (Figure 2). The diffusion of gaseous chlorofluorocarbon molecules ($CFCl_3$, CF_2Cl_2, and CF_3Cl) was tracked using ^{19}F NMR spectroscopy as a way of determining the porosity of the cages. This was supported by the use of PALS, which probes the free volume within materials. The pore diameter estimated by this technique for the porous liquid (6.29 ± 0.08 Å) was consistent with the expected pore diameter of an analogous crystalline cage (6.28 Å).

4. MOC-based composites

MOC-based composites consist of a continuous host matrix in which the cages are physically dispersed. The assembly routes available for composites depend on the relative solubilities ofthe components, but can also depend on the pore structure of the host material. The matrix is classified as ordered or soft amorphous materials.

Dispersion of MOCs in ordered porous materials

The nanometric size of MOCs is ideal for them to be dispersed inside porous materials, such as silica or MOFs. Two main dispersion strategies are used: wet impregnation, and ship-in-a-bottle (Figure 4a). For wet impregnation, the MOC is assembled and then dissolved in a solvent, in which the host material is insoluble. The host porous matrix is then soaked in the MOC-containing solution, the solvent is evaporated, and the MOC becomes embedded in the pores. Using impregnation approaches, Sun and co-workers were able to disperse cuboctahedral MOCs [Cu_{24}(X-bdc)$_{24}$] (X = $NaSO_3$, ^{t}Bu) in mesoporous silica (SBA-15; pore size ≈ 9.7 nm).[39] Loadings of up to 60 wt% were achieved for [Cu_{24}($NaSO_3$-bdc)$_{24}$]. The presence of the MOCs in the pores of the silica caused a decrease in the nitrogen uptake of the composites when compared to the pristine silica, as well as a decrease in the observed pore size. Low loadings of the cage afforded well-dispersed MOCs in the pores, thus presenting good accessibility to their Cu-sites. Therefore the H_2 uptake was enhanced from < 1 to ~20 moles of H_2 per mole of MOC for neat MOC and 10 wt% composite, respectively. An alternative method to track the incorporation of the MOCs in a host material is UV-Vis spectroscopy. H. Deng and co-workers measured the decrease in the absorbance of [Cu_{24}(C_{12}-bdc)$_{24}$] in a chloroform solution as the cage was embedded in IRMOF-74-V (pore size ≈ 4 nm).[40] In contrast, the absorbance of the cage remained nearly constant in the presence of IRMOF-74-IV (pore size ≈ 3 nm), which has a slightly smaller pore size than IRMOF-74-V, indicating that the wet impregnation method is limited by the relative sizes of the pore aperture of the host and the diameter of the cage molecule.

The incompatibility of large cages with small pore apertures can be overcome by a ship-in-a-bottle strategy. Here, the host matrix is soaked in a solution that contains the MOC precursors, to assemble the MOC inside the pores of the host. Wang and co-workers compared both methods by dispersing NH_2-ZrT-1 [$(Cp_3Zr_3O(OH)_3)_4(NH_2\text{-tpa})_6$]$Cl_4$ in the mesoporous MOF DUT-64 (Cp = cyclopentadienyl; NH_2-tpa = 2-aminoterephthalate).[41] The cavities of the MOF (~2.8 nm) are large enough to accommodate the assembled MOC (~2 nm) without the cage leaching through the narrow windows of the framework (≈1.4 nm). Using the ship-in-a-bottle strategy led to higher loading of the MOC (28.2%) than found for wet impregnation (10.3%). Although lower, the apparent loading observed by wet impregnation was not negligible and might arise from cage molecules physically attached to the particles and windows of the framework. The ship-in-a-bottle strategy physically traps the cage inside the host framework, providing a platform for confined-space catalysts. X. Qiu and co-workers confined the octahedral cage [$Pd_6(TPT)_4$] in the mesopores of MIL-101(Fe) (TPT = 1,3,5-Tris(4-pyridyl)-2,4,6-triazine) (Figure 4b).[42] The authors reported an enhanced performance of the MOC@MOF composite for the selective oxidation of benzyl alcohol to benzaldehyde, compared to the pristine MOC (Figure 4c).

Mixed-matrix membranes

Mixed matrix membranes (MMMs) typically consist of an organic polymer (the continuous phase) into which another species (called a filler) is doped to improve upon the performance of the neat membrane, for example improving the selectivity of gas separation.[7] MMMs containing MOCs are usually prepared by mixing solutions of the continuous phase and the MOC under controlled evaporation of the solvent medium (Figure 4d). An alternative method known as “priming” coats particles of the MOC with the polymer before the addition of the remainder of the polymer solution and evaporation. This process can lead to the particles of the filler aggregating, particularly at higher weight loadings. Therefore, many studies of MOCs in MMMs have evaluated the performance of membranes containing a range of weight loadings of the cage, expressed as wt%. In early work using [Cu_{24}(C_{12}-bdc)$_{24}$] as a filler in Matrimid, the excellent solubility of the cage in chloroform enabled weight loadings of as high as 80 wt% to be achieved.[43]

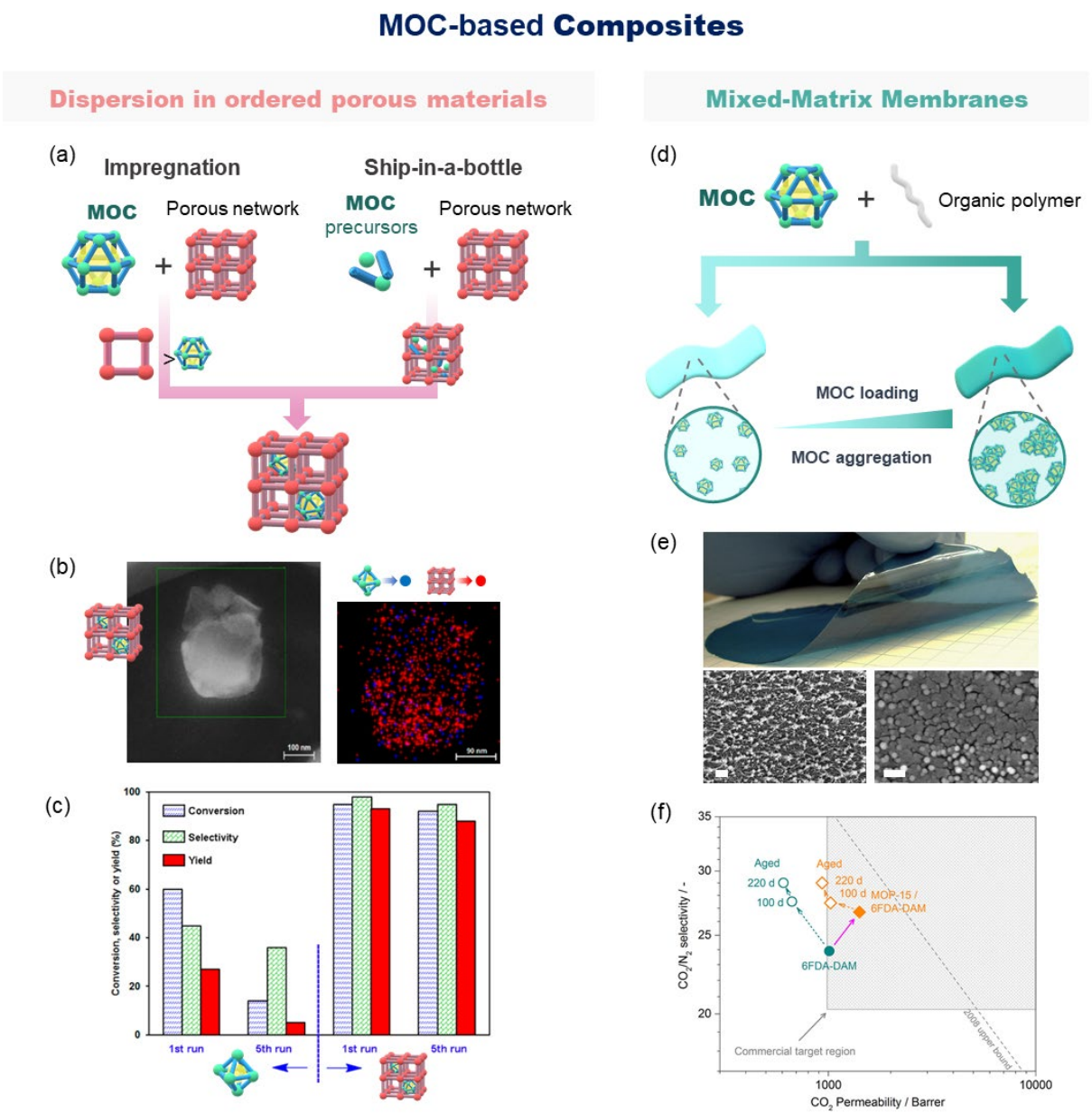

Fig. 4 Strategies to obtain MOC-based composites. (a) Dispersion in ordered porous solids *via* wet impregnation or ship-in-a-bottle. (b) HAADF-STEM image of MOC@MOF composite, elemental analysis showing the Pd from MOC and Cr from MOF. (c) Catalytic performance of MOC vs MOC@MOF composite in benzyl alcohol oxidation. Adapted with permission from ref. 42, Copyright 2016, American Chemical Society. (d) MOC-based Mixed Matrix Membranes (MMM). (e) MOC@polymer MMM, SEM images from cross-sections of 23 and 80 wt% loadings showing defects (scale bar 200 nm). Adapted with permission from ref. 43, Copyright 2014, Elsevier. (f) MOC@polymer MMM performance for CO_2/N_2 separation comparing fresh and aged membranes at 1 bar absolute feed pressure, the 2008 Robeson upper bound showed as reference. Reprinted with permission from ref. 44, Copyright 2018, American Chemical Society.

As the weight loading was increased from 23 wt% to 80 wt%, the aggregation of the MOC particles worsened, and at 80 wt% defects in the form of cracks were observed in the membrane (Figure 4e). These defects are detrimental to selective gas separation. Smoother composites were obtained at lower weight loadings. At a loading of 23 wt%, the gas sorption capacity of the MMMs was superior to both the neat membranes and the neat MOC. From these data, it was inferred that the molecular level dispersity of the MOCs was important because it prevented the long alkyl chains of neighbouring molecules from blocking access to the pores.

Due to the tendency of MOCs to aggregate in the mixing solutions used to fabricate MMMs, their use as fillers often focuses on lower loadings. However, the rate at which the solvent medium is evaporated also induces defects in the obtained MMMs. This was highlighted in work by Liu and co-workers with $[Cu_{24}(NH_2\text{-bdc})_{24}]$ (NH_2-bdc = 5-aminoisophthalate).[44] They dispersed the cage in the polymer 4,4'-(hexafluoroisopropylidene)diphthalic anhydride-

diaminomesitylene (6FDA-DAM) using DMSO as a solvent medium. When lower temperatures and slower drying rates were used to drive off the solvent, the result was that the MOCs agglomerated. When higher temperatures were used, defects were induced in the continuous phase. Finally, an optimum temperature of 373 K was determined for the fabrication procedure. Most notably, the best performing MMM described in this work had a loading of just 1.6 wt% (Figure 4f).

Because the polymer phase in MMMs is flexible, it can encapsulate MOCs in a much tighter fashion than when MOCs are embedded in more rigid hosts. The interaction between the MOC and the polymer is, therefore, more important, and the external functionality of the cage is not the only determinant for solubility. A systematic study of various MOCs embedded in the glassy polymer poly(1-trimethylsilyl-1)propyne (PTMSP) used viscometry to determine the interactions between the cages and the polymer.[45] The viscosity of pre-casting solutions of PTMSP and the cages $[Cu_{24}(C_{12}\text{-bdc})_{24}]$, $[Cu_{24}(^{t}Bu\text{-bdc})_{24}]$, $[Cu_{24}(DEG\text{-bdc})_{24}]$, and $[Cu_{24}(TEG\text{-bdc})_{24}]$ was measured (DEG = diethylene glycol; TEG = triethylene glycol). MOCs with the shorter functional groups ^{t}Bu- and DEG- yielded pre-casting solutions with decreased viscosity, which was attributed to intercalation of the PTMSP polymer into the cages reducing the interaction between the polymer backbones. This work addressed one of the drawbacks of membranes that cages might be able to remediate. The ageing of the polymers causes the backbones to relax and close the pores, leading to a decrease in their permeability, which causes a drop in their gas separation performance. Over the course of one year, all four systems with a weight loading of the MOC of 20 wt% showed a less pronounced loss in the CO_2 permeability than that found for the neat PTMSP membranes. However, the MOCs with shorter chains aged more favourably than TEG-MOC and $[Cu_{24}(C_{12}\text{-bdc})_{24}]$. The worst performing composite was that containing $[Cu_{24}(C_{12}\text{-bdc})_{24}]$, where the long alkyl chains of the cage reduced the free volume of the freshly cast membranes and therefore reduce the permeability by nearly 66%.

5. Cross-linked MOCs

The functionality on MOC surfaces can be used to form chemical bonds that connect the MOCs into extended networks of cross-linked cages. Cross-linking can be implemented at specific points on the backbone of MOCs either through the formation of covalent bonds on the skeleton of the cage or the formation of coordination bonds at labile coordination sites (Figure 5). In both strategies, the MOCs can be considered as a "porous monomer" used to form a polymer. The structural dimensionality of cross-linked MOC materials can be tuned by the structural geometry of MOCs. For instance, a one-dimensional polymeric structure is obtained when only two connection points are used on the surface of MOC, such as on a lantern-type MOC connected through the external axial metal sites. MOCs with polyhedral geometries enable the design of two- or three-dimensional extended networks, in which the cages feature as multiply cross-linked nodes.[46] The branch functionality (f) of the resulting network can be tuned depending on how many covalent and/or coordination sites on the MOC surface participate in the connection. The strategies used to cross-link MOCs can be used to target highly ordered materials or soft matter.

Highly ordered, cross-linked MOCs

Self-polymerisation is the simplest strategy to obtain cross-linked ordered networks. This approach requires cages containing both complementary coordination donor and acceptor moieties.[28, 47] J.-D. Ma, S. Ma and coworkers showed the control over the intercage connectivity by solvent and thermal processing of a MeOH-soluble cuboctahedral cage $[Cu_{24}(OH\text{-bdc})_{24}]$, in which the hydroxy group can coordinate to the axial sites of Cu_2 paddlewheel of neighbouring cages (OH-bdc = 5-hydroxyisophthalate). They reported two coordination polymers: 2D (f = 4) and 3D (f = 6) assemblies.[28] The change from 2D to 3D structures was achieved by the removal of coordination solvents at the axial sites, which triggers further the cross-link of cages between 2D structures. This increase in the dimensionality of the network was reflected by an enhanced CO_2 uptake at 195 K, from ~73 to 130 cm^3/g for the 2D and 3D structures, respectively.

Cross-linking of MOCs with additional, rigid linkers provides crystalline materials, which can be recognised as MOFs. There are two protocols to synthesise such MOFs from discrete MOC units. The simple method is to mix the solution of MOCs with that of additional linkers. For instance, lantern-type MOCs of $[Cu_4(L)_4]$ (H_2L = 3,3'-((2-amino-5-methoxy-1,3-phenylene)bis(ethyne-2,1-diyl)dibenzoic acid) with two copper paddlewheel nodes arranged in an approximately collinear fashion on either side of the MOC cavity were linked by 4,4'-bipyridine to form linear coordination polymers, with branch functionality f = 2.[48] Strictly speaking, although this approach cross-links the MOCs, the one-dimensional polymers themselves are not cross-linked. The synthesis was carried out by adding 4,4'-bipyridine to DMF solutions of the pre-formed MOC. The rigidity of the linker presumably contributed to the formation of a relatively well-ordered polymer, and the structure was determined by single-crystal X-ray crystallography.

Octahedral MOCs based on carbazole-type ligands and copper paddlewheel nodes, $[Cu_{12}(cdc)_{12}]$ (cdc = 9*H*-carbazole-3,6-dicarboxylate), have been used as building blocks (f = 6) in the formation of two-fold interpenetrated MOFs through the reaction of the cage with 4,4'-bipyridine (bpy).[49] Note that the excess addition of pyridine to DEF solutions of $[Cu_{12}(cdc)_{12}]$ caused the MOC to be deconstructed and form a helical one-dimensional coordination polymer. Finally, the use of cuboctahedral MOCs leads to polymers with f = 12, as demonstrated through the use of $[Cu_{24}(H_2N\text{-bdc})_{24}]$ to build the MOF ($[Cu_{24}(NH_2\text{-bdc})_{24}(bpy)_6(H_2O)_{12}]_n$).[50]

The example with octahedral MOC illustrates one of the complications of the coordination bond approach with copper paddlewheels because the MOCs can be prone to disassemble upon variations in pH or in the presence of specific solvents. To overcome the instability of copper paddlewheel nodes, Carné-Sánchez, Maspoch and coworkers used a more stable rhodium

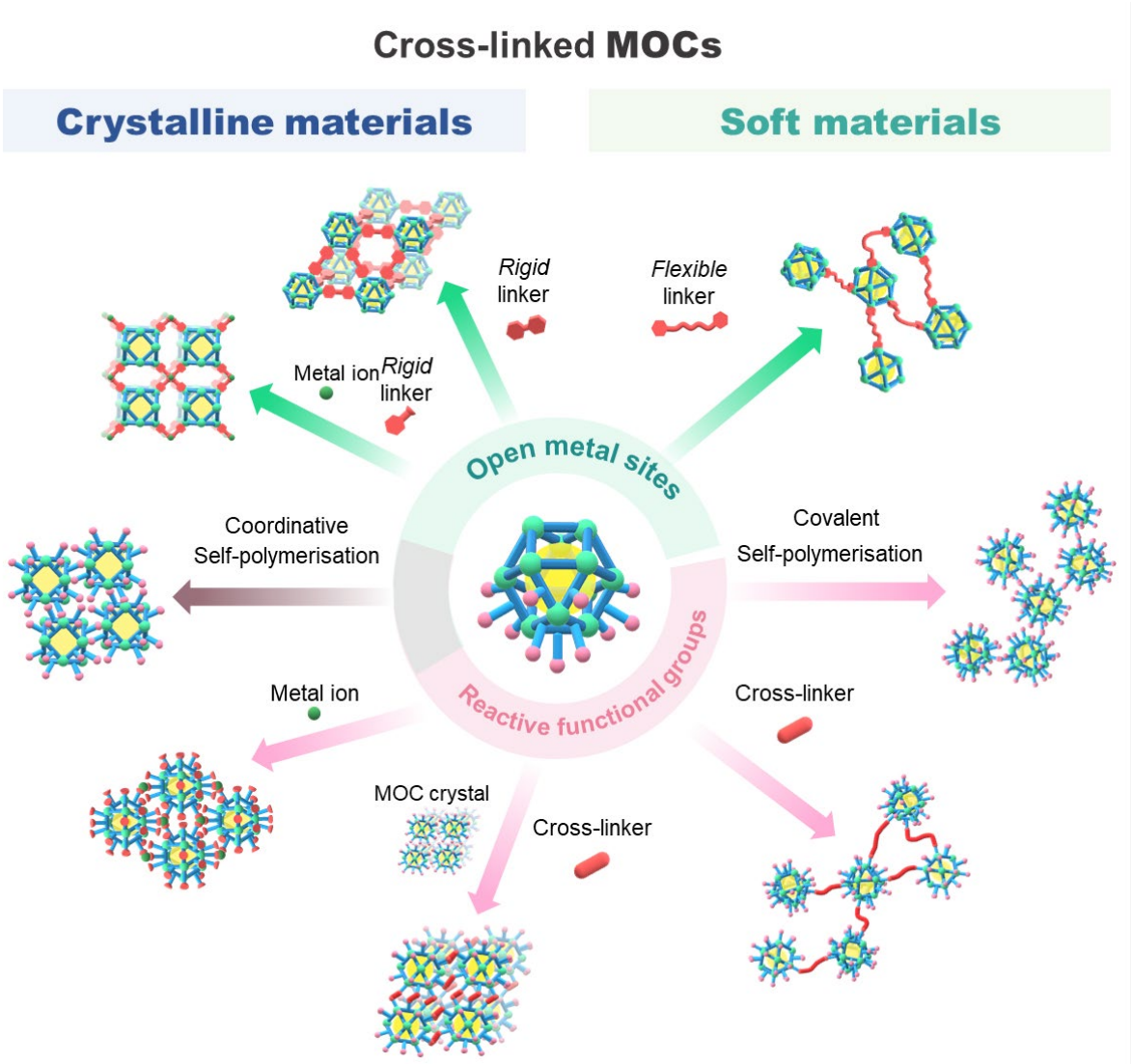

Fig. 5 Strategies to obtain cross-linked MOCs. (top) Cross-linking coordination sites through flexible linkers, rigid linkers, self-polymerisation, or the combination of rigid linker and metal ion. (bottom) Cross-linking through reactive functional groups *via* a crosslinker, self-polymerisation or metal ion.

based cuboctahedral MOC as a building block.[51] Instead of directly connecting them by additional linkers, first the MOC surface was post-synthetically functionalised with polycarboxylates either by introducing carboxylate functionality on isophtalate to form $[Rh_2(COOH\text{-}bdc)_2(H_2O)(DMF)]_{12}$ with a potential branch functionality $f = 24$ or by anchoring isonicotinic acid (HINA) *via* coordination on the rhodium paddlewheel moieties to form $[Rh_2(OH\text{-}bdc)_2(H_2O)(HINA)]_{12}$ with $f = 12$. Then, further reacting these polycarboxylate MOCs with copper ions, mixed metal MOFs were synthesised. The carboxylates from the former $f = 24$ MOC formed trinuclear $Cu_3O(COO)_3$ nodes, leading to the formation of a MOF with **rht** topology. However, due to the charge compensation, the Rh/Cu ratio was identified to be 1:0.75, which implies only 18 carboxylate groups. Thus, the **rht** topology contains charge-induced defects, reducing f to 18. The $f = 12$ MOCs were connected by copper paddlewheels to form a MOF with **ftw** topology. In both cases, the activation process drove them to be amorphous but with permanent porosity originating from the stable rhodium-based MOCs. This was reflected in their maximum N_2 uptake at 77 K, 135 and 250 cm^3/g for **rht** and **ftw** topologies, respectively; whereas for the neat MOC the uptake was ~160 cm^3/g.[13]

While these assembly processes take place in solution, crystal-to-crystal transformations have also been used to link MOCs. Choe and co-workers described a covalent cross-linking that was achieved together with retention of crystalline order, at least in the solvated phase of the materials. The Zr-based MOC ($[Cp_3Zr_3O(OH)_3]_4[NH_2\text{-}tpa]_6[(C_2H_5)_2NH_2]_2Cl_6$; Cp = cyclopentadienyl; NH_2-tpa = 2-aminoterephthalate), was cross-linked through condensation reactions of the pendant amine groups on the MOC with ditopic acyl chloride linkers.[52] They impregnated MOC crystals in a solution of the ditopic linkers, with the reaction occurring in a near single crystal-to-single crystal fashion. The crystalline order of the cross-linked MOCs was confirmed by powder X-ray diffraction measurements, which then showed that order was lost upon activation of the materials. While the pores of the cage molecules were accessible to N_2 at 77 K, the overall uptake of the three cross-

linked materials was inferior (ranging from 75 to 140 cm^3/g) to that of the neat MOC (215 cm^3/g). This is consistent with reduced accessibility to the pores, but the presence of the alkyl chains improved the CO_2 enthalpy of adsorption from ~26 kJ/mol for the neat MOC to a range of 32.2 to 36.3 kJ/mol for the cross-linked MOCs.

Soft matter based on cross-linked MOCs

A straightforward approach to reduce the order of cross-linked MOCs is to connect the cages using cross-linkers with high degrees of freedom. For instance, Shimizu and co-workers covalently cross-linked the MOC $[Cu_{24}(C_{10}\text{-bdc})_{12}(C_8\text{-bdc})_{12}]$ through self-polymerisation at the olefinic groups (C_{10}-bdcH_2 = 5-(dec-9-en-1-yloxy)-isophthalic acid; C_8-bdcH_2 = 5-(octyloxy)-isophthalic acid).[53] The MOC was dissolved in the presence of Grubb's catalyst to drive the olefinic metathesis reaction, yielding insoluble cross-linked polymers. Rheology measurements showed that higher degrees of cross-linking caused increased strain-hardening of the materials. Both the neat MOC and 40% cross-linked MOC were non-porous to N_2 at 77 K. However, the cross-linked MOC displayed improved CO_2 uptake at 195 K (2.18 mmol/g) when compared to the neat MOC (1.16 mmol/g). This increase in porosity is associated with the intercage voids generated by the cross-linking process. An advantage of olefin-functionalised MOCs is that they can undergo both self-polymerisation or cross-linking with another olefin. This is exemplified by the cuboctahedral MOC $[Cu_{24}(C_4\text{-bdc})_{24}]$ (C_4-bdcH_2 = 5-(3-buten-1-yloxy)-isophthalic acid), which can undergo self-polymerisation or copolymerisation with styrene.[54] This copolymer gave shapeable materials and increased their chemical stability, by increasing the hydrophobicity compared to the neat, hydrophilic MOC, and so protected the MOC paddlewheel from decomposition in humid conditions. Additionally, the self-polymerisation process generated an increased extrinsic porosity proved by enhanced CO_2 uptake (from 21 to 40 cm^3/g) and CO_2/CH_4 selectivity (from 23.3 to 48.8) at 273 K.

The use of coordination bonds to incorporate flexible cross-linkers between MOCs has proven to be a useful strategy to form soft materials. In this case, the self-assembly strategy was demonstrated with MOCs based on rhodium paddlewheels. Rhodium paddlewheels are especially good for tracking self-assembly processes as they are relatively stable in solution and show very fine spectroscopic responses to changes in their coordination environment.[55] The MOC $[Rh_{24}(C_{12}\text{-bdc})_{24}]$ was assembled into two macroscopic cross-linked forms through reaction with the ditopic imidazole linker 1,4-bis(imidazol-1-ylmethyl)benzene (bix): one, a gel; the other coordination polymer particles.[56] The extrinsic porosity generated by this approach was observed in the CO_2 adsorption experiments for $[Rh_{24}(C_{12}\text{-bdc})_{24}]$ materials at 195 K, which showed an increase from 46.01 cm^3/g for the neat MOC to values between 57.53 to 70.4 cm^3/g for the MOC-based supramolecular polymers. This method was extended to the MOC $[Rh_{24}(bdc)_{24}]$[57] but this cage required the development of an additional step to solubilise the cage prior to polymerisation.[58] The presence of the dodecoxy chain on the MOC $[Rh_{24}(C_{12}\text{-bdc})_{24}]$ was advantageous for the solubility of the cages, but was less desirable for the gas sorption properties of the soft materials. The microporosity of the polymers based on the MOC $[Rh_{24}(bdc)_{24}]$ was more accessible, resulting in improved gas sorption properties of the materials. This was observed in the N_2 uptake at 77 K of $[Rh_{24}(C_{12}\text{-bdc})_{24}]$ and $[Rh_{24}(bdc)_{24}]$ supramolecular aerogels, increasing from 8 to 38.9 moles of N_2 per mole of MOP, respectively.

6. Conclusion and Outlook

In this tutorial review, we have outlined the currently dominant strategies to synthesise MOC-based porous materials. As molecular porous units, MOCs can be designed and modified to present desired geometries, sizes, and surface functionalities. Once formed, their assembly is determined by intermolecular interactions, in which solvent, ions, organic linkers or polymeric matrices can all play a role. Consequently, control of these interactions allows MOCs to be processed into a wide variety of porous materials, ranging from crystalline solids to liquids. Many opportunities present themselves in the field of MOCs to understand their porous functionality and use them as building blocks for increasingly complex materials where the assembly is controlled over different length scales (Figure 6).

While MOCs can be designed to yield discrete-MOC assemblies with different porous properties, it remains difficult to predict molecular packing in the as-synthesised solid state. In this sense, the field of MOCs lacks the extensive computational work that has been applied to porous organic cages, which would enable targeted synthesis.[59, 60] Nonetheless, there are some approaches to computer-aided cage design and host-guest binding predictions.[61, 62] The development of structure-property relationships in MOCs is also hindered by a lack of structural information for solvent-exchanged polycrystalline phases and activated phases, which is still mostly limited to use of powder X-ray diffraction to illustrate changes in packing.[63] Amorphous, cross-linked MOCs present a greater challenge for their structural characterisation. Here, X-ray scattering techniques including pair distribution function analysis and small-angle X-ray scattering combined with computational simulation should be applied to correlate synthetic conditions and resulting structures.[64]

The molecular nature of MOCs means that there are many ways to increase the complexity of their assemblies, with a simple scheme being to co-assemble at least two different MOCs into one material. Some initial studies have shown that this can be achieved by designing mutual coordination bonds between two different cages;[65] using ionic interactions based on charged MOCs to form MOC-based salts;[66] and mixture of charged MOCs with other molecular species such as polyoxometallates.[67] The possibility of forming molecular salts suggests this approach could be applied to other functional ionic components. Additionally, complexity can be integrated into the same cage by using a multivariate linker strategy, where a controlled ligand diversity leads to different photophysical properties.[68] Tuning the surface functionality of MOCs and interactions between cages in this way would be

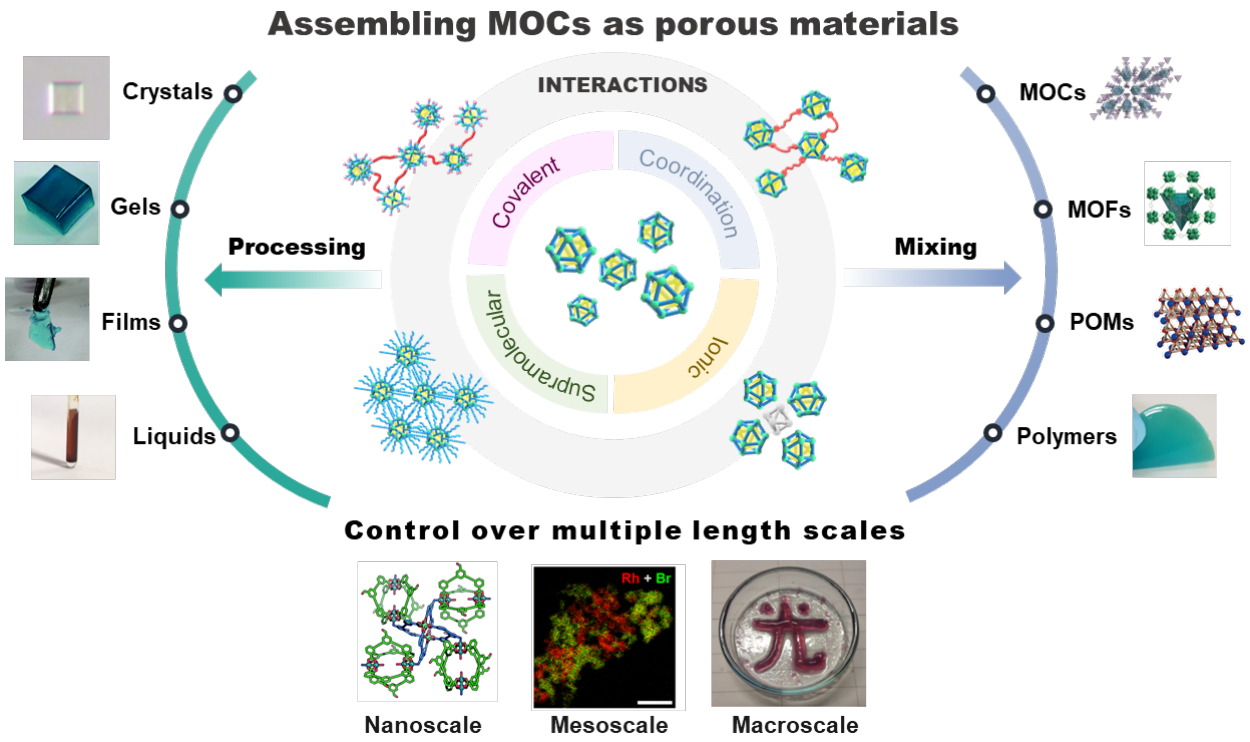

Fig. 6 Assembly routes for MOCs in porous materials: (left) processing into materials, (right) mixing into composites, and (bottom) spatial control over multiple length scales. Reprinted from refs. 36, 52, 54, 65 & 67 with permission from the Royal Society of Chemistry. Reprinted with permission from ref. 38, Copyright 2020, Springer Nature. Reprinted with permission from ref. 41 & 69, Copyrights 2020 & 2018, John Wiley and Sons. Reprinted with permission from refs. 66 & 74, Copyrights 2020 & 2021, American Chemical Society.

relevant not only to molecular assemblies but would also directly impact their miscibility in polymers, enabling improved MMMs (**Section 4**).[69] We anticipate that this approach would extend to porous liquids. Controlling the miscibility of MOCs in liquids is key to obtaining Type 2 porous liquids (solution-type porous liquid) with high MOC loading. Cross-linked MOCs colloids can be also used as porous fillers to form type 3 porous liquids (suspension-type porous liquids). Fine-tuning the interactions between MOCs and matrices would allow for bespoke composites containing combinations of MOCs with high chemical complexities. For instance, the weak interactions between MOCs lead to multiple metastable phases of packing in the solid-state, which directly influence extrinsic porosity. Solvent processing has been shown to switch gate-opening behaviour on and off by causing the formation of one phase over another. Could mechanical stress be used to trigger a phase transition from a metastable packing phase to a more thermodynamically stable phase?[70] This could open the way to mechanotransduction as a means of tuning the gas separation performance in MOC-containing composites such as MMMs.

However, we envisage that the greatest opportunity to increase the complexity of MOC-based materials is to exploit their assembly over different length scales. Considering that MOCs can form cross-linked, mesoscale colloidal particles, chemical heterogeneity can be induced at longer length scales by mixing colloids of distinct cages.[71] Because the individual colloids can be tuned in terms of MOC, intrinsic and extrinsic pore size, degree of cross-linking, porosity, particle size, etc., a huge range of bespoke materials become accessible in which multiple properties may be integrated. Apparently contradictory properties could be integrated into the materials such as hydrophobicity/hydrophilicity, while synergistic effects arising from different MOCs can be anticipated, such as tandem catalysis, selective sensing, controlled release, with similar outcomes expected from composite materials. This allows for the processing of MOCs into multifunctional porous membranes or porous liquids. Increasing length scales also provides the opportunity to investigate the effects of physically induced asymmetry, anisotropy or gradients within the materials, which may enable highly directional functional properties.[72-74] We anticipate that more detailed investigations of assembly mechanisms will enable unusual, out-of-equilibrium phases to be accessed.

Conflicts of interest

There are no conflicts to declare.

Acknowledgements

E. S.-G., M.-Y. T. and J. T. are grateful to the JSPS postdoctoral fellowships for foreign researchers. This study was supported by JSPS KAKENHI Grant Number 18H01995 (Kiban B) and 19H04575 (Coordination Asymmetry) for S.F.

References

1. L. F. Francis, *Materials Processing: A Unified Approach to Processing of Metals, Ceramics and Polymers*, Elsevier Science, 2015.
2. H.-Y. Li, S.-N. Zhao, S.-Q. Zang and J. Li, *Chem. Soc. Rev.*, 2020, **49**, 6364-6401.
3. B. S. Pilgrim and N. R. Champness, *ChemPlusChem*, 2020, **85**, 1842-1856.
4. S. Horike, N. Ma, Z. Fan, S. Kosasang and M. M. Smedskjaer, *Nano Lett.*, 2021, **21**, 6382-6390.
5. I. Stassen, M. Styles, G. Grenci, Hans V. Gorp, W. Vanderlinden, Steven D. Feyter, P. Falcaro, D. D. Vos, P. Vereecken and R. Ameloot, *Nat. Mater.*, 2016, **15**, 304-310.
6. J. Troyano, A. Carné-Sánchez, C. Avci, I. Imaz and D. Maspoch, *Chem. Soc. Rev.*, 2019, **48**, 5534-5546.
7. J. Dechnik, J. Gascon, C. J. Doonan, C. Janiak and C. J. Sumby, *Angew. Chem., Int. Ed.*, 2017, **56**, 9292-9310.
8. R. W. Saalfrank, H. Maid and A. Scheurer, *Angew. Chem., Int. Ed.*, 2008, **47**, 8794-8824.
9. M. Yoshizawa, J. K. Klosterman and M. Fujita, *Angew. Chem., Int. Ed.*, 2009, **48**, 3418-3438.
10. R. Chakrabarty, P. S. Mukherjee and P. J. Stang, *Chem. Rev.*, 2011, **111**, 6810-6918.
11. K. Harris, D. Fujita and M. Fujita, *Chem. Commun.*, 2013, **49**, 6703-6712.
12. E. J. Gosselin, C. A. Rowland and E. D. Bloch, *Chem. Rev.*, 2020, **120**, 8987-9014.
13. A. Carne-Sanchez, J. Albalad, T. Grancha, I. Imaz, J. Juanhuix, P. Larpent, S. Furukawa and D. Maspoch, *J. Am. Chem. Soc.*, 2019, **141**, 4094-4102.
14. S. Lee, H. Jeong, D. Nam, M. S. Lah and W. Choe, *Chem. Soc. Rev.*, 2020, **50**, 528-555.
15. D. W. Zhang, T. K. Ronson, Y. Q. Zou and J. R. Nitschke, *Nat. Rev, Chem.*, 2021, **5**, 168-182.
16. E. Raee, Y. Q. Yang and T. B. Liu, *Giant*, 2021, **5**, 100050.
17. I. Jahović, Y.-Q. Zou, S. Adorinni, J. R. Nitschke and S. Marchesan, *Matter*, 2021, **4**, 2123-2140.
18. D. J. Tranchemontagne, Z. Ni, M. O'Keeffe and O. M. Yaghi, *Angew. Chem., Int. Ed.*, 2008, **47**, 5136-5147.
19. S. Saha, I. Regeni and G. H. Clever, *Coordin Chem Rev*, 2018, **374**, 1-14.
20. J. R. Li, A. A. Yakovenko, W. Lu, D. J. Timmons, W. Zhuang, D. Yuan and H. C. Zhou, *J. Am. Chem. Soc.*, 2010, **132**, 17599-17610.
21. J. Albalad, L. Hernández-López, A. Carné-Sánchez and D. Maspoch, *Chem. Commun.*, 2022, **58**, 2443-2454.
22. J. R. Li and H. C. Zhou, *Nat. Chem,*, 2010, **2**, 893-898.
23. A. Khobotov-Bakishev, L. Hernández-López, C. von Baeckmann, J. Albalad, A. Carné-Sánchez and D. Maspoch, *Adv. Sci.*, Early view, **XX**, 212104753.
24. A. C. Sudik, A. R. Millward, N. W. Ockwig, A. P. Cote, J. Kim and O. M. Yaghi, *J. Am. Chem. Soc.*, 2005, **127**, 7110-7118.
25. S. Torquato and Y. Jiao, *Nature*, 2009, **460**, 876-879.
26. Y. Gong, Y. Zhang, C. Qin, C. Sun, X. Wang and Z. Su, *Angew. Chem., Int. Ed.*, 2019, **58**, 780-784.
27. H. Furukawa, J. Kim, N. W. Ockwig, M. O'Keeffe and O. M. Yaghi, *J. Am. Chem. Soc.*, 2008, **130**, 11650-11661.
28. Z. Niu, S. Fang, X. Liu, J.-G. Ma, S. Ma and P. Cheng, *J. Am. Chem. Soc.*, 2015, **137**, 14873-14876.
29. O. Barreda, G. Bannwart, G. P. A. Yap and E. D. Bloch, *ACS Appl. Mater. Interfaces*, 2018, **10**, 11420-11424.
30. H. Furukawa, J. Kim, K. E. Plass and O. M. Yaghi, *J. Am. Chem. Soc.*, 2006, **128**, 8398-8399.
31. W. M. Bloch, R. Babarao and M. L. Schneider, *Chem. Sci.*, 2020, **11**, 3664-3671.
32. I. Hisaki, C. Xin, K. Takahashi and T. Nakamura, *Angew. Chem., Int. Ed.*, 2019, **58**, 11160-11170.
33. G. Liu, Z. Ju, D. Yuan and M. Hong, *Inorg. Chem.*, 2013, **52**, 13815-13817.
34. M. Zhou, G. Liu, Z. Ju, K. Su, S. Du, Y. Tan and D. Yuan, *Cryst. Growth Des.*, 2020, **20**, 4127-4134.
35. G. A. Craig, P. Larpent, S. Kusaka, R. Matsuda, S. Kitagawa and S. Furukawa, *Chem. Sci.*, 2018, **9**, 6463-6469.
36. K. Omoto, N. Hosono, M. Gochomori and S. Kitagawa, *Chem. Commun.*, 2018, **54**, 7290-7293.
37. M. A. Andrés, A. Carné-Sánchez, J. Sánchez-Laínez, O. Roubeau, J. Coronas, D. Maspoch and I. Gascón, *Chem. - Eur. J.*, 2020, **26**, 143-147.
38. L. Ma, C. J. E. Haynes, A. B. Grommet, A. Walczak, C. C. Parkins, C. M. Doherty, L. Longley, A. Tron, A. R. Stefankiewicz, T. D. Bennett and J. R. Nitschke, *Nat. Chem.*, 2020, **12**, 270-275.
39. L. B. Sun, J. R. Li, W. Lu, Z. Y. Gu, Z. Luo and H. C. Zhou, *J. Am. Chem. Soc.*, 2012, **134**, 15923-15928.
40. H. Deng, S. Grunder, K. E. Cordova, C. Valente, H. Furukawa, M. Hmadeh, F. Gandara, A. C. Whalley, Z. Liu, S. Asahina, H. Kazumori, M. O'Keeffe, O. Terasaki, J. F. Stoddart and O. M. Yaghi, *Science*, 2012, **336**, 1018-1023.
41. B. C. Wang, Z. Y. Feng, B. B. Hao, C. X. Zhang and Q. L. Wang, *Chem. - Eur. J.*, 2021, **27**, 12137-12143.
42. X. Qiu, W. Zhong, C. Bai and Y. Li, *J. Am. Chem. Soc.*, 2016, **138**, 1138-1141.
43. E. V. Perez, K. J. Balkus, J. P. Ferraris and I. H. Musselman, *J. Membr. Sci.*, 2014, **463**, 82-93.
44. X. Liu, X. Wang, A. V. Bavykina, L. Chu, M. Shan, A. Sabetghadam, H. Miro, F. Kapteijn and J. Gascon, *ACS Appl. Mater. Interfaces*, 2018, **10**, 21381-21389.
45. M. Kitchin, J. Teo, K. Konstas, C. H. Lau, C. J. Sumby, A. W. Thornton, C. J. Doonan and M. R. Hill, *J. Mater. Chem. A*, 2015, **3**, 15241-15247.
46. A. V. Zhukhovitskiy, M. Zhong, E. G. Keeler, V. K. Michaelis, J. E. Sun, M. J. Hore, D. J. Pochan, R. G. Griffin, A. P. Willard and J. A. Johnson, *Nat. Chem.*, 2016, **8**, 33-41.
47. G. J. McManus, Z. Wang and M. J. Zaworotko, *Cryst. Growth Des.*, 2004, **4**, 11-13.
48. V. Brega, M. Zeller, Y. He, H. Peter Lu and J. K. Klosterman, *Chem. Commun.*, 2015, **51**, 5077-5080.
49. J. R. Li, D. J. Timmons and H. C. Zhou, *J. Am. Chem. Soc.*, 2009, **131**, 6368-6369.
50. H.-N. Wang, X. Meng, G.-S. Yang, X.-L. Wang, K.-Z. Shao, Z.-M. Su and C.-G. Wang, *Chem. Commun.*, 2011, **47**, 7128-7130.
51. T. Grancha, A. Carné-Sánchez, F. Zarekarizi, L. Hernández-López, J. Albalad, A. Khobotov, V. Guillerm, A. Morsali, J. Juanhuix, F. Gándara, I. Imaz and D. Maspoch, *Angew. Chem., Int. Ed.*, 2021, **60**, 5729-5733.
52. D. Nam, J. Huh, J. Lee, J. H. Kwak, H. Y. Jeong, K. Choi and W. Choe, *Chem. Sci.*, 2017, **8**, 7765-7771.
53. G. Lal, M. Derakhshandeh, F. Akhtar, D. M. Spasyuk, J. B. Lin, M. Trifkovic and G. K. H. Shimizu, *J. Am. Chem. Soc.*, 2019, **141**, 1045-1053.
54. X. Y. Xie, F. Wu, X. Q. Liu and L. B. Sun, *Dalton Trans.*, 2019, **48**, 17153-17157.

55. E. Warzecha, T. C. Berto, C. C. Wilkinson and J. F. Berry, *J. Chem. Educ.*, 2019, **96**, 571-576.
56. A. Carne-Sanchez, G. A. Craig, P. Larpent, T. Hirose, M. Higuchi, S. Kitagawa, K. Matsuda, K. Urayama and S. Furukawa, *Nat. Commun.*, 2018, **9**, 2506.
57. S. Furukawa, N. Horike, M. Kondo, Y. Hijikata, A. Carné-Sánchez, P. Larpent, N. Louvain, S. Diring, H. Sato, R. Matsuda, R. Kawano and S. Kitagawa, *Inorg. Chem.*, 2016, **55**, 10843-10846.
58. A. Carné-Sánchez, G. A. Craig, P. Larpent, V. Guillerm, K. Urayama, D. Maspoch and S. Furukawa, *Angew. Chem., Int. Ed.*, 2019, **58**, 6347-6350.
59. E. O. Pyzer-Knapp, H. P. G. Thompson, F. Schiffmann, K. E. Jelfs, S. Y. Chong, M. A. Little, A. I. Cooper and G. M. Day, *Chem. Sci.*, 2014, **5**, 2235-2245.
60. L. Turcani, R. L. Greenaway and K. E. Jelfs, *Chem. Mater.*, 2019, **31**, 714-727.
61. A. Tarzia and K. E. Jelfs, *Chem. Commun.*, 2022, **58**, 3717-3730.
62. T. A. Young, R. Gheorghe and F. Duarte, *J. Chem. Inf. Model.*, 2020, **60**, 3546-3557.
63. S. P. Argent, I. da Silva, A. Greenaway, M. Savage, J. Humby, A. J. Davies, H. Nowell, W. Lewis, P. Manuel, C. C. Tang, A. J. Blake, M. W. George, A. V. Markevich, E. Besley, S. Yang, N. R. Champness and M. Schröder, *Inorg. Chem.*, 2020, **59**, 15646-15658.
64. Z. Wang, C. Villa Santos, A. Legrand, F. Haase, Y. Hara, K. Kanamori, T. Aoyama, K. Urayama, C. M. Doherty, G. J. Smales, B. R. Pauw, Y. J. Colón and S. Furukawa, *Chem. Sci.*, 2021, **12**, 12556-12563.
65. A. W. Markwell-Heys, M. Roemelt, A. D. Slattery, O. M. Linder-Patton and W. M. Bloch, *Chem. Sci.*, 2022, **13**, 68-73.
66. A. J. Gosselin, G. E. Decker, A. M. Antonio, G. R. Lorzing, G. P. A. Yap and E. D. Bloch, *J. Am. Chem. Soc.*, 2020, **142**, 9594-9598.
67. B. Le Ouay, H. Yoshino, K. Sasaki, Y. Ohtsubo, R. Ohtani and M. Ohba, *Chem. Commun.*, 2021, **57**, 5187-5190.
68. D. Nam, J. Kim, E. Hwang, J. Nam, H. Jeong, T.-H. Kwon and W. Choe, *Matter*, 2021, **4**, 2460-2473.
69. Y. N. Yun, M. Sohail, J.-H. Moon, T. W. Kim, K. M. Park, D. H. Chun, Y. C. Park, C.-H. Cho and H. Kim, *Chem. - Asian J.*, 2018, **13**, 631-635.
70. J. Troyano, A. Legrand and S. Furukawa, *Trends Chem.*, 2021, **3**, 254-265.
71. M. Y. Tsang, S. Tokuda, P.-C. Han, Z. Wang, A. Legrand, M. Kawano, M. Tsujimoto, Y. Ikeno, K. Urayama, K. C. W. Wu and S. Furukawa, *ChemRxiv*, 2021. DOI: 10.33774/chemrxiv-2021-6dhhs
72. A. Legrand, G. A. Craig, M. Bonneau, S. Minami, K. Urayama and S. Furukawa, *Chem. Sci.*, 2019, **10**, 10833-10842.
73. A. Legrand, Z. Wang, J. Troyano and S. Furukawa, *Chem. Sci.*, 2021, **12**, 18-33.
74. A. Legrand, L.-H. Liu, P. Royla, T. Aoyama, G. A. Craig, A. Carné-Sánchez, K. Urayama, J. J. Weigand, C.-H. Lin and S. Furukawa, *J. Am. Chem. Soc.*, 2021, **143**, 3562-3570.